An Inversion Method for the Determination of the Internal Structure of Latex Particles from Fluorescence Nonradiative Energy Transfer Experiment

Elías Pérez[†] and Jacques Lang*

Institut Charles Sadron, CNRS-ULP Strasbourg, 6, rue Boussingault, 67083 Strasbourg Cedex, France

Received: July 2, 1998; In Final Form: October 15, 1998

A method is presented for the determination of the internal structure of core−shell latex particles from fluorescence nonradiative energy transfer between a donor and an acceptor chemically bonded to the polymer chains which are supposed to form the core (donor) and the shell (acceptor) of the particles. The method is based on the assumption that these two types of polymer chains are radially distributed inside the particles. The distributions of the polymer labeled with the donor and with the acceptor are directly obtained from the analysis of the fluorescence decay curve of the donor, using a least-squares method coupled with a regularization condition, given the so-called regularization technique of inversion. In the inversion method there is no model and no analytical expression used to describe the concentration profiles of the polymers. We show how this method was tested with known polymer concentration profiles, from which fluorescence decay curves were first constructed and then analyzed. The original polymer distributions were accurately recovered. We show also, with real examples, how this method can give useful information on the internal structure of core−shell particles after their synthesis performed under various conditions, and after annealing of the particles.

Introduction

Latex particles with a core−shell structure are of considerable practical and economical importance. A great number of studies have been undertaken to determine their internal structure or to elucidate the correlation between their microscopic structure and their properties, as for instance their mechanical properties. Core−shell latex particles are accessible by emulsion polymerization, mostly by two-step emulsion polymerization. It is known, however, that perfect core−shell latex particles are usually difficult to obtain, for example when the thermodynamic incompatibility between the core polymer and the shell polymer is not high enough.

Several methods have been employed for the determination of the shape and the internal structure of core−shell latex particles. Among these methods, transmission electron microscopy was the most widely used.[1] With this technique a contrast between the polymer which is supposed to form the core (core polymer) and the polymer which is supposed to form the shell (shell polymer) of the particle is necessary. This contrast is either natural or can be obtained for instance by staining one of the two polymers. However, when the two polymers are too close chemically, the contrast is difficult to obtain. Other methods were employed for the study of the internal structure of core−shell latex particles, as for example small-angle neutron scattering using perdeuterated monomers in the second step of the polymerization,[1j,2] or small-angle X-ray scattering, analyzed directly[3] or by a contrast variation method.[4] Solid-state nuclear magnetic resonance was also employed, based on the difference in T_g between the two polymers.[5] Finally, light scattering[6] was also used to investigate the internal structure of core−shell latex particles, and dynamical spectroscopy measurements,[1b,c,7] atomic force microscopy,[8] differential scanning calorimetry,[1c] and titration of functional groups at the surface or in the shell[9] also gave arguments for the existence of structured core−shell latex particles. We have been interested in finding a new method, more general, and, in particular, utilizable to the determination the internal structure of core−shell latex particles made of very similar polymers (identical T_g, same affinity to staining components).

Recently, investigations of the internal structure of core−shell latex particles were performed using fluorescence nonradiative energy transfer (NRET).[10−12] The principle is to label, during polymerization, the core polymer with an energy donor (acceptor), and the shell polymer with an energy acceptor (donor). If a perfect core−shell structure is synthesized, no energy transfer occurs, or, more precisely, only a very small energy transfer occurs through the interface between the core and the shell. If the core polymer and the shell polymer have interdiffused for some raison, during or after the synthesis, then energy transfer between the donor and the acceptor occurs. This energy transfer shows up on the time-resolved fluorescence emission of either the donor or the acceptor. From the analysis of the fluorescence decay, and with the aid of a geometrical model, information on the internal structure of the particles was obtained. In two of the studies mentioned above,[10,11] the model proposed earlier by Winnik and co-workers[13] for the study of the further gradual coalescence of particles in latex films has been adopted. In this model (see below) the particles present three concentric domains: one forming the core, another forming the shell, and the third in the middle where core polymer and shell polymer are homogeneously mixed. This model was improved by using an analytical expression for the distribution of the donor and of the acceptor labeled polymer chains.[12] In this model, which is more realistic, a smooth sigmoidal distribution of the donor and of the acceptor inside the particle was assumed. Using the adjustable parameters appearing in the sigmoidal equation, the theoretical decay curve could be satisfactorily fitted to the experimental decay. From this fit a reasonable estimate of the concentration profile of the

[†] Present address: Fakultät für Physik, Universität Konstanz, Fach M696, D-78464 Konstanz, Germany.

10.1021/jp982855s CCC: $18.00
Published on Web 03/11/1999

core polymer and the shell polymer inside the particles was obtained.

In the above studies by NRET, the determination of the internal structure of core−shell latex particles rests on the assumption of a geometrical model of distribution of the donor- and acceptor-labeled polymer chains. In the first model, the distribution of the polymers which is imposed seems clearly far from the reality (we will see that it give, however, very reliable, although global, information on the internal structure). The second model is closer to the reality but the distribution of the donors and the acceptors are nevertheless, to some extent, also imposed. We have already discussed elsewhere[12] the possibility of using a Fickian distribution for the donors and the acceptors inside the core−shell particles. However, the great number of kinetic and diffusive effects that seemed involved in the synthesis of the core−shell particles led us to discard the choice of a Fickian distribution of the core polymer and the shell polymer inside the particles. For all these reasons, we have elaborated a new method for the determination of the distribution profile of the core polymer and of the shell polymer inside core−shell latex particles that we have applied to the study of some core−shell latex particles. In this method, the distributions of the donor- and the acceptor-labeled polymer chains are directly deduced from the fluorescence decay curve without any model chosen a priori. However, to recover the concentration profiles directly from the fluorescence decay curves, two hypotheses were made. The first one was to assume a radial symmetry of the concentration profile, and the second one a continuity in the variation of the concentration as a function of the radial coordinate, r. This last hypothesis means that the concentration profile behaves smoothly. These hypotheses seem reasonable and are mainly justified by the way the core−shell particles studied here were synthesized. A two-step semicontinuous emulsion polymerization was employed. First, the core of the particle was synthesized and next the shell was polymerized around the core. It was checked that no second nucleation occurred during the synthesis and that the particle surface was smooth. Details concerning the synthesis and the control of the particles shape are given elsewhere.[11] A final remark concerns the boundary condition of the radial distribution: the derivative of the concentration with respect to r is zero at $r = 0$ and at $r = R_P$, the radius of the particle. This is because on both coordinates there is no mass flux: the center is a point of symmetry, and the border is closed to mass transfer.

This article is organized in the following way. We start by giving the first-order nonlinear integral equation that relates the fluorescence intensity to the concentration profile. This equation is next introduced in a weighted least-squares procedure, where the theoretical fluorescence decay is best fitted to the experimental one. In this procedure, the fluorescence equation, containing the unknown concentration profile, is solved using the theory of inversion. This leads, finally, to the concentration profile of the polymer chains. This concentration profile is obtained, therefore, without the aid of any analytical equation. The method is next tested using three different, known, concentration profiles: a rather flat, a rather sharp, and an intermediate concentration profile. Finally, the method is employed to determine the internal structure of some synthesized core−shell latex particles, and the results are compared to those obtained[11] for the same particles, with the more simple model employed by Winnik and co-workers for the studies of latex film formation[13] and core−shell particles internal structure.[10]

General Equation of the Fluorescence Decay

The normalized decay of the intensity of the fluorescence emitted by the donors from a system which contains N_D donors, with a spatial concentration, $C_D(r)$, surrounded by a spatial concentration, $C_A(r)$, of acceptors, after excitation, is given by the following temporal equation:

$$\frac{i(t)}{i_M} = \frac{e^{-t/\tau}}{N_D}\int C_D(\mathbf{r}) \exp[-qC_A(\mathbf{r})(t/\tau)^{1/2}]\, dr \qquad (1)$$

where i_M is the maxima intensity of the fluorescence decay curve, τ is the fluorescence lifetime of the donor, and q is a quantity related to the nonradiative energy transfer process, given by

$$q = \frac{4}{3}\beta\sqrt{\pi}\cdot\pi R_0^{\,3} \qquad (2)$$

In eq 2, β is an orientation factor and R_0 is the Förster distance. The orientation factor, β, takes into account the relative orientation of the dipoles of the donors and of the acceptors during the energy transfer. If the molecules are static during the fluorescence process, which is a condition satisfied in our case (the fluorescence measurements are performed at a temperature below the polymers T_g), β takes the numerical value of 0.8452.[14] The Förter distance R_0 is the distance between the donor and the acceptor at which the donor has an equal probability to transfer its energy by dipolar resonance to the acceptor, or to lose it by fluorescence emission. For the couple donor−acceptor (phenanthrene−anthracene) employed in our study, R_0 is equal to 2.3 nm, whereas the Förter distance for phenanthrene−phenanthrene energy transfer is equal to 0.877 nm which makes the phenanthrene−phenanthrene energy transfer negligible compared to the phenanthrene−anthracene energy transfer, even at the relatively high fluorophore concentration employed in our study, $C_0 = 0.0699\ \text{nm}^{-3}$ (see below). Indeed, at this concentration the efficiency of the energy transfer, which is given by the relation $E = R_0^6/(R_0^6 + r^6)$, is only 0.22% for phenanthrene−phenanthrene energy transfer compared to 42% for phenanthrene−anthracene energy transfer.

Notice that the integration of eq 1 applies to the whole volume of the sphere. Equation 1 represents the contribution of each differential element of the system to the total fluorescence intensity. Each contribution has the original form proposed by Förster,[15] but now the concentration of the donor and of the acceptor depends on the position of the differential elements. This generalization is valuable because R_0 is much lower than the radius of the latex particles, which is between 85 and 148 nm in our study.

Equation 1 is applicable when the system is excited by a very short excitation pulse, analogous to a Dirac function. In general, the excitation pulse does not have the shape of a Dirac function when compared to the probe fluorescence lifetime. Its width cannot be neglected, and the emitted fluorescence intensity is, in fact, the convolution of the proper fluorescence decay of the probe, $i(t)$, with the excitation pulse. This convolution is written as

$$I(t) = I_M\int_0^t f(t-\xi)i(\xi)\, d\xi \qquad (3)$$

where I_M is the maxima of the fluorescence decay curve. We will consider the form of the excitation pulse in our calculations. Notice that if $f(t-\xi)$ is a delta function, eq 3 reduces to eq 1.

The fluorescence intensity depends on the distribution of both the donor and the acceptor. However, if one supposes, as is the

case in our latex particles, a total occupation of the space by the polymer chains, independent of their labeling, these two distributions are related through the equation

$$C_D(\mathbf{r}) + C_A(\mathbf{r}) = C_0 \tag{4}$$

where $C_0/2$ is the donor or acceptor concentration in the limit of a total mixing, and also with the condition that the system contains the same number of donor and acceptor, which is the case in the latex particles studied here.[11]

We can write the general expression of the fluorescence intensity in a more convenient form if we define two kernels:

$$K_F(\xi,C_D(r)) = \exp\left[-\frac{\xi}{\tau} - qC_A(r)\left(\frac{\xi}{\tau}\right)^{1/2}\right] = \exp\left[-\frac{\xi}{\tau} - qC_0\left(1 - \frac{C_D(r)}{C_0}\right)\left(\frac{\xi}{\tau}\right)^{1/2}\right] \tag{5}$$

$$K(t,C_D(\mathbf{r})) = \int_0^t K_F(\xi,C_D(r))f(t-\xi)\,d\xi \tag{6}$$

In eq 5 we have introduced eq 4 to express $C_A(r)$ as a function of $C_D(r)$, and used the hypothesis of a radial symmetry. The first kernel, eq 5, is directly related to the process of NRET, and the second one, eq 6, is the convolution of eq 5 with the excitation pulse. These kernels allow us to write the fluorescence intensity in the following form:

$$\frac{I(t)}{I_M} = \frac{4\pi}{N_D}\int_v K(t,C_D(r))C_D(r)r^2\,dr \tag{7}$$

Equation 7 is an integral equation where the concentration profile, $C_D(r)$, is unknown. $K(t,C_D(r))$ is the Kernel of the integral transformation. The integral equation is non linear because the kernel also depends of the unknown concentration $C_D(r)$.

Equation 7 is the integral equation from which the concentration profile, $C_D(t)$, will be obtained without any predetermined model. To get the concentration profile, eq 7 will be introduced in a least-squares procedure and solved using the method of inversion described now.

Methodology of the Inversion

We will inverse eq 7 using a least-squares method coupled with a regularization condition. This procedure does not assume any concentration profile and gives the spatial distribution profile of the emitted probes, directly from the fluorescence intensity decay curve. This is the reason why this method is called regularization technique of inversion. This technique has already been used in different other situations where it appeared to be very powerful to obtain, for example, the molecular weight distribution of polymers from the photon correlation spectroscopy,[16] to recover the fluorescence lifetime distribution of pyrene adsorbed on dehydroxylated silica gel surface,[17] and to recover the acceptor concentration distribution in the NRET experiments,[18] when the acceptor is either attached to polymer chains diffusing across an interface or free in a polymer matrix where aggregation between donors and acceptors occurs, or when donor and acceptor are adsorbed on the surface of a polymeric microsphere. However, it is the first time, to our knowledge, where this method is applied to the analysis of the fluorescent data to obtain directly the spatial distribution of the fluorescent groups inside latex particles. Nevertheless, the method proposed here for the determination of the internal structure of latex particles is general and can be applied to other nonlinear problems of inversion.

The method consists, essentially, in the introduction of an additional condition to eq 7 which describes the fluorescence decay of an excited probe, called the regularization condition, and which helps to solve the inversion problem. This condition must take into account the characteristics of the systems studied, which are known or which can reasonably be assumed. This simplifies the search of the solution and also highly improves the confidence in the solution. In our case, one can reasonably assume a continuity in the concentration profile of the polymer chains inside the particles, which results from the experimental conditions used for the synthesis of the particles.[11]

We start to build the functional χ-square of eq 7, which is given by eq 8:

$$\chi^2[C_D(r)] = \frac{1}{\nu}\int_{t_1}^{t_2} w(t)\left\{I_e(t) - \frac{4\pi}{N_D}\int_v K(t,C_D(r))C_D(r)r^2\,dr\right\}^2 dt \tag{8}$$

where ν is the number of degrees of freedom defined later, $w(t)$ is a weighting function, $I_e(t) = I(t)/I_M$ represents the experimental normalized fluorescence intensity, and t_1 and t_2 are the times which determine the limits of the values of $I_e(t)$ used for the inversion. In our study, the spatial integration is only applied to the volume of the individual latex particle. Indeed, except in the special cases where latexes were dissolved in THF to make films (see below), the fluorescence decay curves were recorded with the latex particles in dispersion and there is no energy transfer between adjacent latex particles in this case since the mean distance between adjacent particles is very large (high dilution[11]) compared to the diameter of the latex particles, and the Förster distance, R_0, very low compared to the diameter of the particles.

The weighting function, $w(t)$, is given by the dispersion, $\delta I(t)$, of the value of the fluorescence intensity around its average value at each time, t, of the fluorescence decay curve:

$$w(t) = 1/(\delta I(t))^2 \tag{9}$$

In the single-photon-counting experiments this dispersion is given by[19]

$$\delta I(t) = [I(t)]^{1/2} \tag{10}$$

The inversion consists to find the concentration $C_D(r)$ which minimizes χ^2. However, the minimization of χ^2 without any other additional condition gives rise to a solution which is not stable. This is a consequence of the experimental origin of $I(t)$ and is a classical ill-conditioned problem.[20] Indeed, due to the noise in the experimental data some rows in the inversion matrix (see below) are nearly similar and the matrix then becomes singular. The introduction of the regularization condition eliminates this singularity [20,22,23] and leads to a solution that is stable to weak variations in $I(t)$. This condition is given by eq 11:

$$\Omega[C_D(r)] = \int_0^{R_p}\left[\frac{d^2C_D(r)}{dr^2}\right]^2 dr^2 \tag{11}$$

which will be minimized at the same time as χ^2. The minimization of this functional gives a concentration profile, $C_D(r)$, which is continuous until the second derivative.[21] This equation forces the least-squares procedure to give a smooth concentration profile. This satisfies the experimental conditions employed for

the synthesis of the particles, which is, as already mentioned, a regular growth of the latex particles which are built successively with the donor and then with the acceptor-labeled polymer chains. It must be remarked that irregular jumps are indeed observed in the concentration profiles when the regulation condition is not applied.

In addition to eq 11, another condition must be introduced in the least-squares procedure, which is the mass conservation. We have to impose that, during the process of inversion, the number of donors inside the particle stays constant and equal to the one introduced in the particles during the synthesis. To take into account this condition we define the following functional:

$$M[C_D(r)] = \left[1 - \frac{4\pi}{N_D}\int_0^{R_p} C_D(r) r^2 \, dr\right]^2 \tag{12}$$

which strictly should be zero.

Notice that the mass conservation given by eq 12 is a physical condition, while the continuity of C_D(r), imposed by eq 11, is a kind of hypothesis concerning the shape of the distribution since it excludes solutions leading to irregular or hilly concentration profiles.

Finally, eq 8 together with eqs 11 and 12 give the following functional which has to be minimized to get the best fit of the theoretical decay to the experimental one:

$$R^2[C_D(r)] = \chi^2[C_D(r)] + \lambda'_m M[C_D(r)] + \lambda'_r \Omega[C_D(r)] \tag{13}$$

In eq 13 λ'_m and λ'_r are two Lagrange multipliers; λ'_r is also called regularization parameter. The role of the Lagrange multipliers is to weight the contribution of each condition in the minimization of R^2. These parameters are very important in the inversion procedure. They cannot take any value and must be related to the experimental conditions to obtain a correct inversion. They are determined simultaneously with $C_D(r)$ during the minimization of R^2. We will see in the next section that λ'_m is related to the accepted mass error (this is done in eq 26), while λ'_r is related to the experimental data (see eqs 28−31). In this way λ'_m and λ'_r are directly related to the experiments. They are calculated at the same time that the concentration profile and are not imposed.

Numerical Equations

We minimize eq 13 by an iterative method, mainly because of the non linearity of the kernel in eq 7. In addition, the determination of λ'_r is also iterative, as we will see below. For this calculation we introduce the discrete and dimensionless concentration, c_k, defined as

$$c_k = C_D(r_k)/C_0 \tag{14}$$

where r_k is the k point of the discrete radial position. The discrete form of eq 13 is then

$$R^2 = \frac{I_M}{\nu}\int_{t_1}^{t_2} \frac{1}{I_e(t)}\left\{I_e(t) - \frac{C_0}{N_D}\int_k K(t,c_k) c_k 4\pi r_k^2 \Delta r_k\right\}^2 dt + \frac{I_M}{\nu}\lambda_m\left[1 - \frac{C_0}{N_D}\int_k c_k 4\pi r_k^2 \Delta r_k\right]^2 + \frac{I_M}{\nu}\lambda_r \sum_k \sum_l c_k H_{kl} c_l \tag{15}$$

where $\int_k$ represents the trapezoidal rule used as quadrature in the spatial integration, λ_m and λ_r are the precedents lagrange multipliers devised by I_M/ν, and H_{kl} is the matrix which gives the second derivative of $C_D(r)$ with respect to r in a discrete form. H_{kl} is expressed as[23]

$$H = \begin{bmatrix} 1 & -2 & 1 & 0 & 0 & 0 & 0 & \cdots & 0 \\ -2 & 5 & -4 & 1 & 0 & 0 & 0 & \cdots & 0 \\ 1 & -4 & 6 & -4 & 1 & 0 & 0 & \cdots & 0 \\ 0 & 1 & -4 & 6 & -4 & 1 & 0 & \cdots & 0 \\ \vdots & & & \ddots & \ddots & \ddots & & & \vdots \\ 0 & \cdots & 0 & 1 & -4 & 6 & -4 & 1 & 0 \\ 0 & \cdots & 0 & 0 & 1 & -4 & 6 & -4 & 1 \\ 0 & \cdots & 0 & 0 & & 1 & -4 & 5 & -2 \\ 0 & \cdots & 0 & 0 & & & 1 & -2 & 1 \end{bmatrix} \tag{16}$$

which supposes equally spaced points along the radial coordinate. Notice that λ_r also contains the factors of normalization of this discrete second derivative.

H is a square matrix $n_i \times n_i$, where n_i is the number of points, c_k, recovered in the inversion process. This matrix also satisfy the boundary condition

$$\partial C_D/\partial r = 0 \tag{17}$$

at $r = 0$ and $r = R_p$ which is appropriate for our problem.

A necessary condition to minimize eq 15 is that the first derive with respect to c_j must be equal to zero, which means that

$$\frac{\partial R^2}{\partial c_j} = -2\frac{I_M}{\nu}\beta_j = 0 \tag{18}$$

where β_j is defined as

$$\beta_j = b_j^0 - N_j^0 + [b_j^1 - N_j^1]c_j + \lambda_m\left[1 - \frac{C_0}{N_D}\int_k c_k 4\pi r_k^2 \Delta r_k\right] - \lambda_r \sum_k H_{jk} c_k \tag{19}$$

where b_j^0, b_j^1 and N_j^0, N_j^1 are defined in the Appendix and are not necessary for the rest of the discussion. The roots of eq 19 are determined by the Newton−Raphson method.[24] We need therefore the derivative of eq 19 with respect to c_j and c_k, which is

$$\frac{\partial^2 R^2}{\partial c_j \partial c_k} = 2\frac{I_M}{\nu}\alpha_{jk} \tag{20}$$

where

$$\alpha_{jk} = 2\{K_{jk}^0 + (c_j + c_k)K_{jk}^1 + c_j c_k K_{jk}^2\} + 2\lambda_m + \lambda_r H_{jk} \tag{21}$$

where the matrix K_{jk}^0, K_{jk}^1, and K_{jk}^2 are also defined in the Appendix.

The Newton−Raphson method gives therefore the following equation:[24]

$$\sum_k \alpha_{jk}\delta c_k = \beta_j \tag{22}$$

where δc_k is a element of the increment vector, δc, defined by

$$\mathbf{c}^n = \mathbf{c}^{n-1} + \delta\mathbf{c} \tag{23}$$

$\mathbf{c}^n$ is the ensemble of the new concentrations calculated from the preceding approximation $\mathbf{c}^{n-1}$. We denote the initial guess as $\mathbf{c}^0$. $\delta\mathbf{c}$ is obtained from the resolution of eq 22. We can write the solution of eq 22 as

$$\mathbf{c}^n = \mathbf{c}^{n-1} + \alpha^{-1}\cdot\beta^{n-1} \tag{24}$$

Finally, we will establish two equations to determine the Lagrange multipliers.

We can use eq 19 in the convergence limit to determine λ_m. In this limit, β_j tends to zero and therefore $\sum_j \beta_j$ tends also to zero. We use the identity

$$\sum_j \sum_k H_{jk} c_k \equiv 0 \tag{25}$$

to establish the expression of the first Lagrange multiplier, in the convergence limit, which is therefore

$$\lambda_m = \frac{1}{n_i \epsilon_m} \sum_j (b_j^0 - N_j^0 + [b_j^1 - N_j^1] c_j) \tag{26}$$

where ϵ_m is the tolerance imposed to the mass conservation, defined as

$$\epsilon_m = |1 - \frac{1}{N_D} \int_v C_D(r) 4\pi r^2 \, dr| \tag{27}$$

In our calculation we have imposed the value of 0.01 to this quantity.

The second Lagrange multiplier, λ_r, will be determined from the definition of χ^2, eq 8. After a first iteration, done in order to minimize R^2, the ensemble of c_k depends of λ_r and thus χ^2 becomes also a function of λ_r. We use the following function

$$\gamma(1/\lambda_r) = \left[\int_{t_1}^{t_2} \frac{1}{I_e(t)} \left\{ I_e(t) - \frac{C_0}{N_D} \int_k K(t, c_k(1/\lambda_r)) c_k 4\pi r_k^2 \Delta r_k \right\}^2 \right]^{1/2} \tag{28}$$

to establish an equation to determine λ_r. We can observe that γ and χ^2 are related by

$$\chi^2 = (I_M/\nu)\gamma^2 \tag{29}$$

We use the analytical properties of $\gamma(1/\lambda_r)$, proposed by Badeva and Morazov,[22] to determine the parameter λ_r. These authors have shown, from the theory of inversion by the regularization technique, that $\gamma(1/\lambda_r)$ is a concave decreasing function. This allows to calculate λ_r by a Newton−Raphson method, which is written as

$$\frac{1}{\lambda_r^n} = \frac{1}{\lambda_r^{n-1}} - \frac{R\,(1/\lambda_r^{n-1})}{R'(1/\lambda_r^{n-1})} \tag{30}$$

where R is also a concave decreasing function defined as

$$R = \gamma(1/\lambda_r) - \delta \tag{31}$$

where δ is the tolerance for γ. The numerical value of δ is determined from eq 29 as follows. From the χ^2 distribution, we know that a reasonable value for χ^2 is the unity. Indeed, $\chi^2 \approx 1$ indicates that the distribution calculated from the inversion method has a probability near 0.5 to be a good distribution,[25] while a typical value for I_M is 15 000. On the other hand, we will see, in the application section, that the number of degrees of freedom, ν, takes the value of 23. Therefore, an appropriate value for γ^2 is approximately 0.001. As a consequence, we have imposed in our calculation the value $\sqrt{0.001}$ to the tolerance δ. In this way, R goes to zero in each iteration and χ^2 approximates to unity. The derivative of R with respect to $1/\lambda_r$ takes the form

$$R'(1/\lambda_r) = \frac{\lambda_i \lambda_r}{\gamma(1/\lambda_r)} \{ \sum_j c'_j (b_j^0 - N_j^0) 4\pi r_j^2 \Delta r_j + \sum_j c'_j c_j (b_j^1 - N_j^1) 4\pi r_j^2 \Delta r_j \} \tag{32}$$

where c'_j represents the derivative of c_j with respect to λ_r, calculated from eq 22. If we suppose that the main dependence of α_{jk} with λ_r comes from the term $\lambda_r H_{jk}$, then the derivative of eq 22 with respect to λ_r gives

$$\sum_k \alpha_{jk} \delta c'_k = -\sum_l H_{jk} \delta c_k \tag{33}$$

where δc_k is the solution of eq 22. Therefore, the solution of eq 33 is given by

$$(\mathbf{c}')^n = (\mathbf{c}')^{n-1} - \alpha^{-1}\cdot(H\cdot\delta\mathbf{c}) \tag{34}$$

We see that in order to solve eqs 22 and 33 the same inverse matrix α^{-1} is used.

The matrix α is inverted by the method of singular value decomposition.[26] This method allows to eliminate the small singular values which are associated to experimental errors, and avoids propagating the errors during the iterative process used to calculate **c**.

We can resume the iterative process of inversion as follows:

1. First, a concentration profile, $\mathbf{c}^0$, is chosen which is described by 33 values of c as a function of the coordinate r. $n_i = 33$ is a number large enough to obtain a good definition of the concentration profile and to avoid calculation which would consume too much time. A first value for λ_r is also chosen. The value $\lambda_r = 1$ turns out to be a good estimate. Finally, as first guess for $\mathbf{c}'$, $(\mathbf{c}')^0 = \mathbf{c}^0$ is used.

2. Using **c** we calculate λ_m with eq 26. Next, we calculate β and α from their definition, given by eqs 19 and 21, respectively. We also calculate R from eqs 28 and 31.

3. Equation 22 is solved to obtain $\delta\mathbf{c}$, using the inverse matrix, α^{-1}. From the values of $\delta\mathbf{c}$, together with the same inverse matrix α^{-1}, a new value for $\mathbf{c}'$ and thus a value for R' are obtained using eqs 34 and 32, respectively. Then, a new value for λ_r can be calculated from eq 31. At the same time one gets, from eq 24, a new ensemble of values for **c**.

4. The iterative process is continued, beginning from step 2, until a minimal value of R^2 (eq 15) is found. For all the results presented here, R^2, as function of the number of iterations, reaches a minimal and constant value.

Finally, it must be noted that two additional conditions were introduced into the process of iteration. A condition that limits the value of c_k and says that c_k must be less than, or equal to, 1, the maximum value possible for c_k: if c_k is greater that 1, we impose $c_k = 1$, an absorbing condition. The other condition is a reflecting condition which avoids negative values of the concentration: if c_k is less than zero we impose $c_k = c_{k-1}$, which is not negative. Both conditions do not fix the values of the concentration because they can be modified in the next iteration. These conditions are necessary to have a physical, meaningful, solution at the end of the inversion.

Simulation

We show now how the inversion method presented above was tested. The principle is to recover a known concentration profile. The known concentration profile is used to generate a fluorescence decay curve. This decay curve is next analyzed with the least-squares procedure which includes the inversion

calculation. This leads to a concentration profile which can be then compared to the original one. This comparison will indicate if the proposed method is reliable or not.

The simulated concentration profile was obtained by assuming a Fickian diffusion of two components labeled differently with donor and acceptor fluorescent groups. These components with their bonded fluorescent groups form originally a perfect core−shell particle. However, as diffusion of the components inside the particles takes place, the concentration profile flattens, and the flattening increases with time. This is described by the following equations.

The initial concentration of a perfect core−shell particle is written as

$$c_k(r) = 1 \qquad \text{if } 0 \le r \le R_c \tag{35}$$

$$c_k(r) = 0 \qquad \text{if } R_c \le r \le R_p$$

where R_c is the radius of the core. The concentration profile as function of time for a Fickian diffusion is given by[27]

$$c(r) = \frac{1}{2} + \frac{2}{R_p r}\sum_{k=1}^{\infty} e^{-D\alpha_k^2 t}\frac{\alpha_k^2 R_p^2 + 1}{\alpha_k^2 R_p^2}\sin(\alpha_k r)\int_0^{R_p} r c_k(r) \sin(\alpha_k r)\, dr \tag{36}$$

where D is the diffusion coefficient and α_k represents the roots of the equation

$$R_p\alpha_k \mathrm{ctg}(R_p\alpha_k) - 1 = 0 \tag{37}$$

whose solution can be found elsewhere.[28]

Equation 36 is the solution of the diffusion equation with the boundary conditions $\frac{\partial c(r)}{\partial r} = 0$, for $r = 0$ and $r = R_p$, the situation considered in the H matrix definition (eqs 16 and 17). The solution of the diffusion equation satisfies, by definition, the mass conservation. One can also observe that in the limit of $t \to \infty$, $c(r) = {}^1/_2$, which is also the case in the method of inversion presented before, where we assumed $C_A = C_D = C_0/2$ for a complete mixing.

The concentration profile is generated numerically. For this, the 50 first terms from eq 36 are taken and each generated concentration profile is identify by the product Dt.

The excitation pulse is also modeled. We use the following expression proposed by Demas:[19]

$$f(t) = f_m(e^{-at} - e^{-bt}) \tag{38}$$

where $f_m = 80$, $a = 8/\tau$, $b = 80/\tau$, and $\tau = 46$ ns. This gives an excitation pulse width at middle high of 6 ns.

For each concentration profile, the simulated fluorescence decay curve is obtained from eq 7 using 257 points separated by 0.36 ns. Next, a Gaussian noise is added to each of these points, which is a good approximation of the noise present after a great duration of accumulations of the emitted fluorescence. The relative amplitude of the noise is approximately 3% for the points close to the maximum of the curve and 6% for the lowest points. This roughly reproduces the experimental conditions. We use for the inversion the points located between the maximum of the decay curve, corresponding to time t_M, and the time $t = \tau$ ($\tau = 46$ ns) after this maximum, which corresponds to a total of 128 points. The part of the decay curves comprising the time between t_M and $t = t_M + \tau$ corresponds to the domain where the fluorescence intensity presents the lowest noise. This is the reason why this part of the decay was chosen to minimize the functional R^2 . When using the points below the maximum and above $t_M + \tau$, the inversion method is less stable and, therefore, the convergence much longer to obtain. A tolerance on the total concentration of the donors of 1% ($\epsilon_m = 1\%$, eq 27) is imposed, and 33 values of the concentration profile are finally obtained after the least-squares and the inversion calculations.

In applying the inversion procedure to the simulated fluorescence decay curves, only the two first terms of eq 15 were used. The reason is that it was not necessary to smooth the recovery curve of distribution; in these cases the program converges very easily toward a regular, continuous, profile. This indicates that, indeed, the regularization method is necessary only because of the imperfection of the experimental decay curve.

The program of inversion was tested for various situations; three of them are reported here. In the first one the donor and acceptor groups are almost completely mixed. In this case the distribution curve (curve 1 in Figure 1) was obtained with $Dt = 3000$ nm^2. The second corresponds to an intermediate case between a perfect core−shell structure and a total mixing. In this case the curve of distribution (curve 1 in Figure 2) was obtained with $Dt = 1000$ nm^2. The third corresponds to a more marked profile. The distribution curve (curve 1 in Figure 3) was obtained in this case with $Dt = 100$ nm^2. From these three profiles of concentration we calculated the three fluorescence decay curves (curve 2) shown in Figures 1−3. This was done by introducing eqs 36 and 37 into eq 7 (where $C_D(r) = (C_0)$-$c(r)$ and q is given by eq 2), and by adding the noise to each decay curve. The method of inversion was then applied to the fluorescence decay curves using the region of the decay marked in bold on the figures. In Figures 1−3 are also represented the first guess of the concentration profile used in each case. They are given by curves 3. Finally, after the program was run, we recovered the concentration profiles represented by the vertical bars in Figures 1−3.

In the two first cases (Figures 1 and 2) the agreement between the original profile (curve 1) and that obtained with the inversion method (vertical bars) is very satisfactory. In the last case (Figure 3) the agreement is less satisfactory, although the profile obtained is very close from the starting profile. It is possible that a better agreement will be obtained by increasing the number of values used to describe the concentration profile in this case. Indeed, in the region where the profile presents a great variation the number of concentration values is not large enough to give a very precise description of the profile.

Two remarks must still be made. The first one is that the convergence of the final profile (vertical bars in Figures 1−3) toward the starting profile (curve 1 in Figures 1−3) is obtained only if the initial profile (curve 3 in Figures 1−3) is not too far from the solution. The second is that the convergence could be appreciated, directly by comparison with the initial profile, on the one hand (comparison between curve 1 and the vertical bars in Figures 1−3), and by examining the asymptotic value of R^2, which decreased and reached a constant value, during the successive iterations, on the other hand. In the real cases there is no known initial profile and the convergence is, therefore, appreciated from the asymptotic behavior of R^2 only.

Application

The method of inversion has been applied to the analysis of the decay curves obtained for the core−shell latex particles labeled with phenanthrene in the core and anthracene in the shell. The particles were made of an equal volume of core and

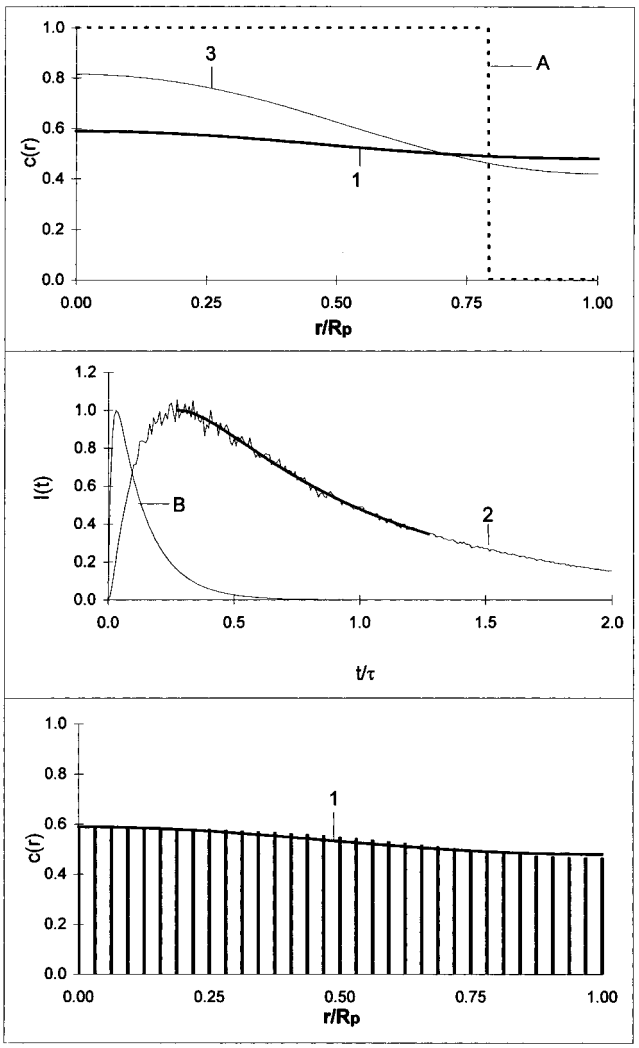

Figure 1. Curve 1: Simulated distribution profile of a donor-labeled component obtained assuming a Fickian diffusion process with $Dt = 3000$ nm^2. Curve 2: Simulated fluorescence decay of the donor distributed inside the particle according to curve 1. Curve 3: Initial distribution of the donor used in the least-squares and inversion procedure. Vertical bars (figure on the bottom): Distribution concentration profile of the donor-labeled component recovered after applying of the method of inversion to the fluorescence decay curve (curve 2). (A) Donor concentration profile for a perfect core−shell particle. (B) Flash used for the simulation of the fluorescence decay (curve 2).

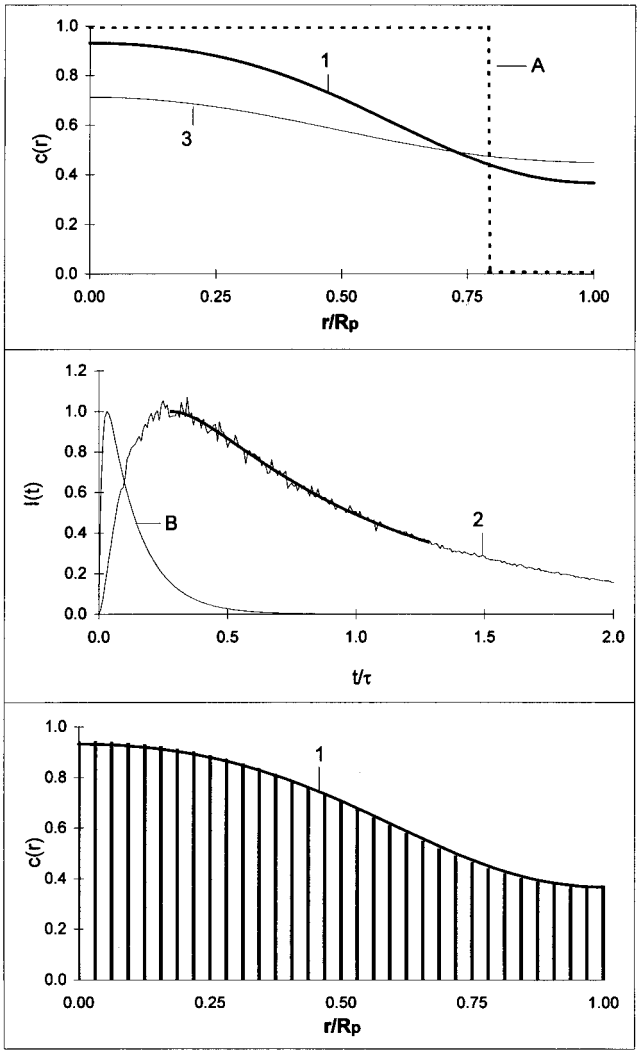

Figure 2. Curve 1: Simulated distribution profile of a donor-labeled component obtained assuming a Fickian diffusion process with $Dt = 1000$ nm^2. Curve 2: Simulated fluorescence decay of the donor distributed inside the particle according to curve 1. Curve 3: Initial distribution of the donor used in the least-squares and inversion procedure. Vertical bars (figure on the bottom): Distribution concentration profile of the donor-labeled component recovered after applying of the method of inversion to the fluorescence decay curve (curve 2). (A) Donor concentration profile for a perfect core−shell particle. (B) Flash used for the simulation of the fluorescence decay (curve 2).

shell polymer. Some characteristics of these latexes, which were synthesized earlier,[11] are given in Table 1, and typical fluorescence decay curves are reported in Figure 4. These curves show that most of the information concerning energy transfer appears at times above the maximum of the decay curves. This indicates that the fact of applying the inversion method only above the maximum of the decay curve, for the practical reason indicated in the simulation section, is perfectly justified. As already mentioned above, the fluorescence decay curves were previously[11] analyzed using the model proposed by Winnik and coworkers.[13] This model rests on the assumption that the donor and the acceptor are situated in three distinct regions of the particle (see Figure 5), and that the donor fluorescence emission comes from the two regions where the donors are far from any acceptor (region 1 in Figure 5), and where the donors are surrounded by a constant concentration of acceptors (region 2 in Figure 5). Energy transfer occurs in this last region only. A fraction of mixing between the chains labeled with the donor and with the acceptor was measured using this model. This fraction of mixing, f'_A, could be obtained from the area under the fluorescence decay curves, according to the following equation:[11]

$$f'_A = (A - A_D)/(A(\infty) - A_D) \tag{39}$$

where A is the area under the decay curve corresponding to the actual particle, A_D is the area under the decay curve corresponding to latex labeled with the donor only, and $A(\infty)$ is the area under the decay curve obtained from a film where the donor- and the acceptor-labeled polymer chains are completely mixed. Although this model is very simple compared to the inversion method, it gave useful information on the distribution of the polymer chains in the expected core−shell latex particles after their synthesis.[10,11] However, we will see that more information on the internal structure of the latex particles is obtained from the inversion method.

To correctly carry out the inversion of the decay curves it was necessary to use the three terms in eq 13, and not only the

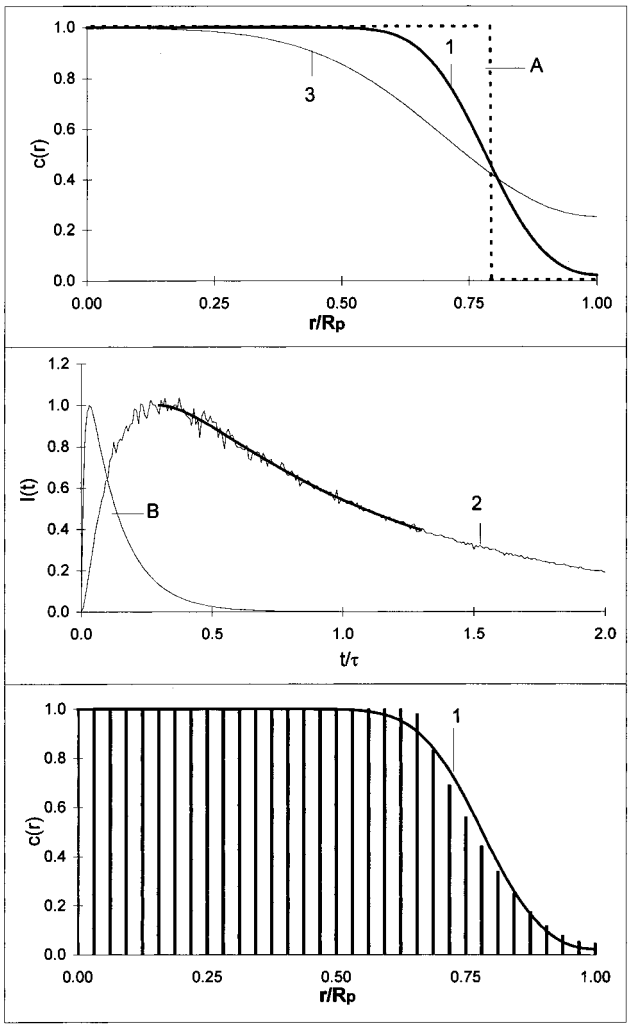

Figure 3. Curve 1: Simulated distribution profile of a donor-labeled component obtained assuming a fickian diffusion process with $Dt = 100$ nm^2. Curve 2: Simulated fluorescence decay of the donor distributed inside the particle according to curve 1. Curve 3: Initial distribution of the donor used in the least-squares and inversion procedure. Vertical bars (figure on the bottom): Distribution concentration profile of the donor-labeled component recovered after applying of the method of inversion to the fluorescence decay curve (curve 2). (A) Donor concentration profile for a perfect core−shell particle. (B) Flash used for the simulation of the fluorescence decay (curve 2).

two first one as in the case of the simulations. The use of the two first terms only brings about discontinuous concentration profiles. The condition of regularization (eq 11) proved also to be necessary for a good stability of the convergence.

The value of the concentration C_0, which appears in eq 15, was obtained from the analyze of the decay curve for two films prepared from a solution of core−shell latex particles dissolved in THF. One of the latexes was the latex CS1 and the other the latex CS4 (see Table 1). Since both latexes contain the same number of donors and acceptors and since the mixing between donors and acceptors is total, one has $C_A = C_D = C_0/2$, and the decay equation becomes

$$\frac{i(t)}{i_M} = \exp\left[-\frac{t}{\tau} - q\frac{C_0}{2}\left(\frac{t}{\tau}\right)^{1/2}\right] \qquad (40)$$

where q (eq 2), τ, the lifetime of the donor (phenanthrene, $\tau =$ 46 nm), and the excitation pulse are known. The same value for C_0 was obtained with both films, $C_0 = 0.0699$ nm^{-3}.

With the exception of the latexes dissolved in THF employed to prepare films, all the latexes have been studied in the form of dispersion, even those which were annealed.

Before each fluorescence decay curve was recorded, the flash of excitation was recorded. Neither the curve of the flash nor the decay curve was smoothed before the inversion. The decay curve and the excitation pulse are given on the left-hand side in Figures 6−8 for the various systems (dispersion or film) studied. For the inversion procedure, 56 points located between the maximum of the curve (t_1) and the point corresponding to time $t = \tau$ after the maximum (t_2) were used (zone marked in bold on the decay curves, recomputed from the distribution profile obtained after inversion). This defines $n_t = 56$ as the number of points used in the inversion calculation. The process of iterations was stopped when the value of R^2 became very weak and constant. Two examples are given in Figure 9 which show that, although the inversion procedure is applied to a limited part of the decay curve, the entire decay curve from $t = 0$ to $t = 2\tau$, recomputed from the distribution profile, fits perfectly well the experimental decay. These good fits result from the fact that, in the least-squares procedure and in the reconstruction of the decay curve, the convolution involves the data from $t = 0$ (and not only from t_1) to t_2.

The results of the analysis of the decay curves obtained for films prepared after dissolution of latexes CS1 and CS4 in THF are given in Figures 6C and 7C. The distribution of the donor, represented by the vertical bars in the corresponding figures, is perfectly horizontal. This result is as expected since dissolution of the latexes in THF leads to a homogeneous distribution of the donor and acceptor labeled polymer chains.

The analysis of the fluorescence decay curves recorded from the dispersions, containing either native or annealed latex particles, was done in the following way. First, the distribution of the donor in the particles annealed during the longest period of time, Δt_a, was analyzed, using as first estimate the distribution found in the film formed from dissolution of the latex in THF. Next, the distribution curve of the donor in the particles annealed during the period of time $\Delta t_b < \Delta t_a$ was determined, using as first estimate the distribution obtained for the latex annealed during the period of time Δt_a, and so on until the distribution of the donor in the native particles was obtained. Doing so, the estimates were relatively close from the true values and the convergence of the program was usually much faster than when other estimates for the distribution of the donor were chosen.

The evolution of the concentration profile of the donor in the particles CS1, native and annealed at 140 °C for 1, 3, 7, and 16 h, and of the particles CS4, native and annealed at 90 °C for 16, 85, and 183 h, has been determined. We give here only some of the distribution profiles obtained.

The distributions of the donors in latexes CS1 and CS4 after their synthesis (native) are given on the right-hand side in Figures 6A and 7A, respectively. Comparison between these distributions (vertical bars) and the distribution for perfect core−shell particles (dashed lines) shows that in both cases perfect core−shell particles have not been synthesized. This result is in agreement with the results obtained from our previous analysis[11] in which the fraction of mixing, f'_A, was determined. Indeed, Table 1 shows that the values of f'_A obtained previously using eq 39 are different from zero, whereas they should be equal, or close to, zero (no mixing) if perfect core−shell particles would have been synthesized. Moreover, a fraction of mixing, f_i, between donor- and acceptor-labeled polymer chains can be

TABLE 1. Characteristics of the Latex Studied, Figure Number where the Donor-Labeled Polymer Chains Concentration Profile is given, Parameter χ^2 Measuring the Quality of the Fit, Mass Recovered after the Inversion Procedure, Fraction of Mixing, f'_A, obtained from the Model in Figure 5, and Fraction of Mixing, f_i, calculated from the Distribution Profile (Vertical Lines) of the Donor-Labeled Polymer Chains shown in Figures 6−8

latex	core−shell	figure	χ^2	mass	f'_A	f_i
CS1: native	PMMA−PMMA	6A	2.548	0.992	0.484	0.599
CS1: 7 h at 140 °C	PMMA−PMMA	6B	4.444	0.990	1.000	0.822
CS1: THF[a]	PMMA−PMMA	6C	0.442	0.990	1.000	1.000
CS4: native	PBMA−PBMA	7A	1.446	1.004	1.000	0.909
CS4: 85 h at 90 °C	PBMA−PBMA	7B	1.099	1.000	1.000	0.922
CS4: THF	PBMA−PBMA	7C	0.511	0.990	1.000	1.000
CS2: native	PBMA−PMMA	8A	1.714	0.995	0.391	0.564
CS3: native	PBMA−Poly(MMA-*co*-BMA)	8B	1.773	0.988	0.521	0.599
CS7: native; core cross-linked	PBMA−PBMA	8C	2.953	0.984	0.758	0.827

[a] THF = tetrahydrofuran.

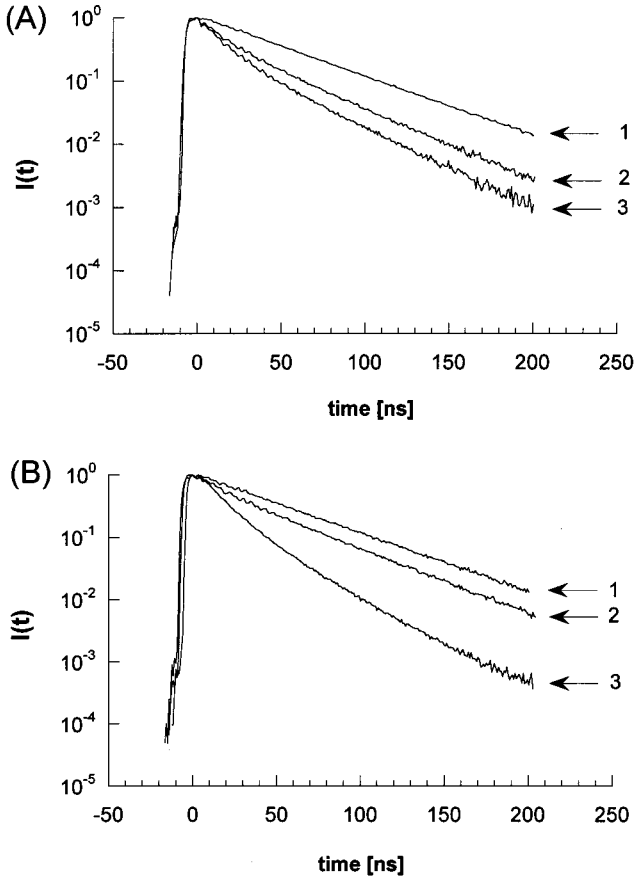

Figure 4. Fluorescence decay curves of phenanthrene (donor). Curves 1 in parts A and B are monoexponential decay curves of phenanthrene in the absence of anthracene (acceptor) in PBMA (A) and PMMA (B) latex particles, respectively. Curves 2 and 3 in part A are for the native PBMA−PBMA core−shell particles CS7 and CS4 (see Table 1), respectively. Curves 2 and 3 in part B are for the native PMMA−PMMA core−shell particles CS1 (see Table 1) and for the same particles after dissolution in THF and film formation, respectively. In particles CS1, CS4, and CS7, phenanthrene has been introduced in the core and anthracene in the shell during the synthesis (see ref 11). Notice that in each example the fluorescence emission decays over more than 4 times the phenanthrene fluorescence lifetime (46 ns).

calculated from the distribution curves (vertical bars) of the donors inside the particles shown in Figures 6A and 7A. These values of f_i are also reported in Table 1. Comparison between f'_A and f_i for the native particles of latexes CS1 and CS4 indicates that the trend is the same: the fraction of mixing increases when one goes from CS1 to CS4. This result has already been discussed previously and explained by the fact that the polymerization temperature (80 °C) is much higher than the T_g (32 °C) of PBMA (latex CS4), whereas the T_g (110 °C)

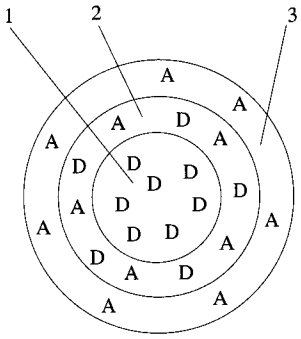

Figure 5. Schematic representation of the model with three distinct regions containing uniform concentrations of the donor- and of the acceptor-labeled polymer chains. Regions 1 and 3 contain only donor- and acceptor-labeled polymer chains, respectively. Region 2 contains a mixture of donor- and acceptor-labeled polymer chains. Energy transfer occurs only in region 2, and the donor fluorescence intensity comes from regions 1 and 2.

of PMMA (latex CS1) is higher that the temperature of polymerization. Thus, in the case of latex CS4 chains of PBMA can migrate inside the core of the particles during the synthesis of the shell and the fraction of mixing is very high, close to 1, whereas in the case of latex CS1 only some acceptors, monomers of MMA, and oligomers of PMMA can migrate in the core where they polymerize during the synthesis of the shell, and the fraction of mixing between the core and the shell polymers is in this case much less, close to 0.5.

The distribution of the donor in latexes CS1 and CS4 after annealing (7 h at 140 °C for latex CS1, and 183 h at 90 °C for latex CS4), is given on the right-hand side in Figures 6B and 7B, respectively. One sees that the distribution profile of the donor is smoother than in the native particles and that some acceptors are now present at the center of the particles. In these cases also the values of f'_A and f_i (see Table 1) are satisfactorily close.

We show, on the right-hand side in Figure 8, the donor distribution curves in latexes CS2, CS3, and CS7 (see Table 1). These three latexes contain PBMA in the core and are in the native form. The shell of latex CS2 is made of PMMA, that of latex CS3 is a copolymer of MMA and BMA (25/25 vol/vol), and that of latex CS7 is made of PBMA, but the core of latex CS7 is cross-linked.[11] None of these particles present a perfect core−shell structure. However, one can notice some differences between them and with the native latexes CS1 and CS4. For instance, while going from particles CS4 native (Figure 7A) to particles CS2 native (Figure 8A), the domain containing only donor-labeled polymer chains widen around the center of the particles. This is due to the partial thermodynamic incompatibility between PBMA and PMMA, which shows up in the synthesis of latex CS2, and which does not exist for latex CS4,

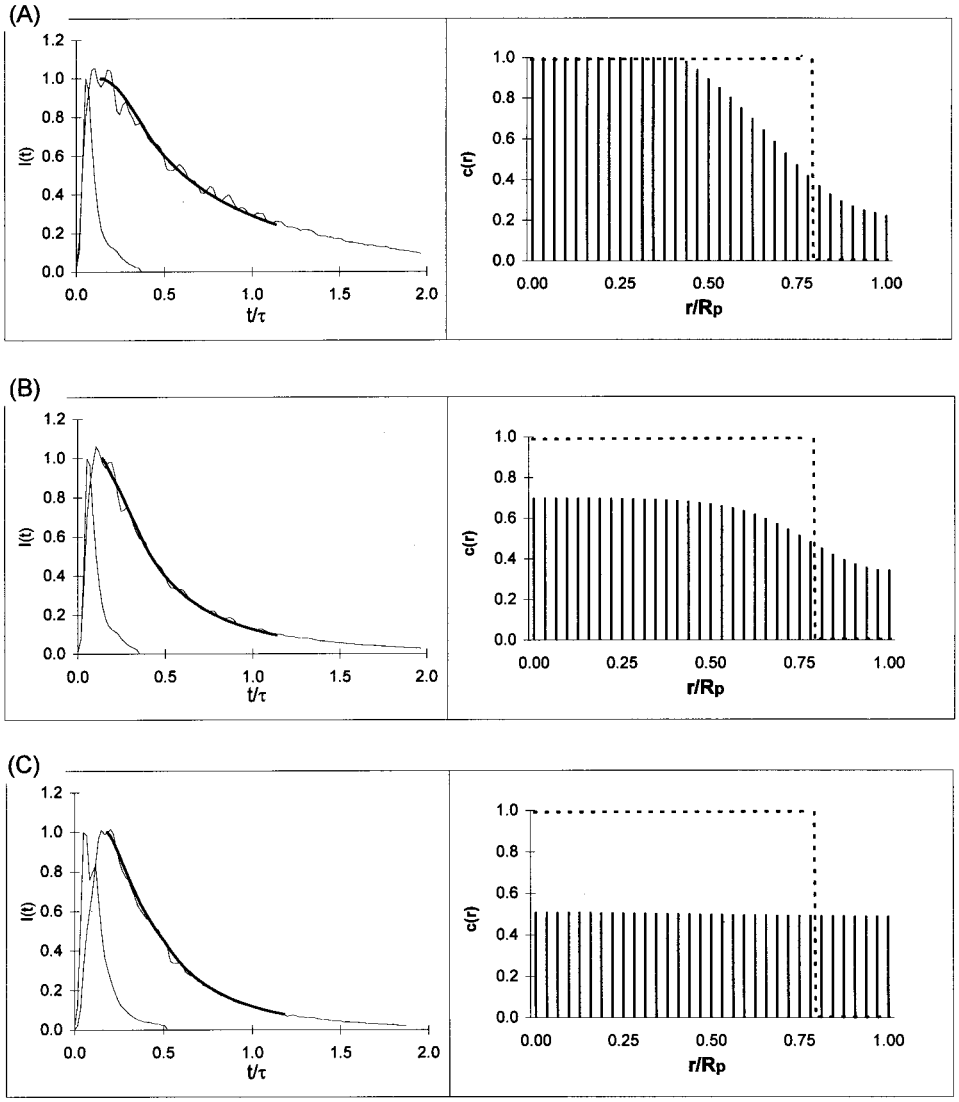

Figure 6. Latex particles CS1: (A) native; (B) annealed at 140 °C for 7 h; (C) film after dissolution in THF. Left-hand side: Experimental flash and experimental fluorescence decay. Bold: Region of the fluorescence decay where the least-squares and inversion procedure was applied. Right-hand side: Distribution profile of the donor-labeled polymer chains obtained with the least-squares and inversion procedure (vertical bars) and theoretical distribution corresponding to a perfect core−shell structure (dashed lines).

made of the same polymer, PBMA, in the core and in the shell. Another interesting observation which can be made concerns latexes CS4 and CS7. Both latexes contain PBMA in the core and in the shell, but, as said above, the core of the latex CS7 is cross-linked. This explains why the region where the donor is not mixed with any acceptor is extended in the case of particles CS7 (Figure 8C) compared to the case of particles CS4 (Figure 7A). However, one can wonder why this difference is not larger. That is due to the fact that, here again, acceptors, monomers of BMA and oligomers of PBMA can migrate in the core where they polymerize during the synthesis of the shell. The migration of these small molecules is not prevented enough by the cross-linking of the core of the particles.

Various remarks are still to be made concerning the curves shown in Figures 6−8. Let us notice first that the concentration profile of the acceptor results directly from that of the donor using eq 4. Let us notice next that the decays in bold, superimposed on the experimental fluorescence decay curves on the left-hand side in Figures 6−8, have been calculated using eq 7, starting from the concentration profiles of the donor and of the acceptor, obtained by the method of inversion. One can see that there is a good agreement between the experimental fluorescence decay curves and those recomputed from the distribution curves obtained by the method of inversion. On the other hand, it must be recalled that all our particles contain an equal volume of polymer labeled with the donor and of polymer labeled with the acceptor. Due to this composition the theoretical concentration profile of the donor, which is represented in dashed lines in Figures 6−8, appears disymmetrical along the particle radius. Being spherical particles, the theoretical limit between the core and the shell is located at a distance from the center of the particle close to the 8/10 of the particle radius. This remark is important since mistakes can be made if one considers just the concentration profiles shown on the figures, ignoring the distribution of the polymer in space. One could believe, for example, that the distribution obtained for the native particles CS4 (Figure 7A) is characterized by a relatively weak fraction of mixing between donors and acceptors since the region which contains only donors seems rather important. This region, however, represents a weak fraction in volume of the particle, and the fraction of mixing is in fact very high, as seen also from the values of f'_A and f_i reported in Table 1. In Table 1 we present the value of χ^2 given by eq 8, where ν is the number of degree of freedom for the adjustment. In our case $\nu = n_t - n_i$,

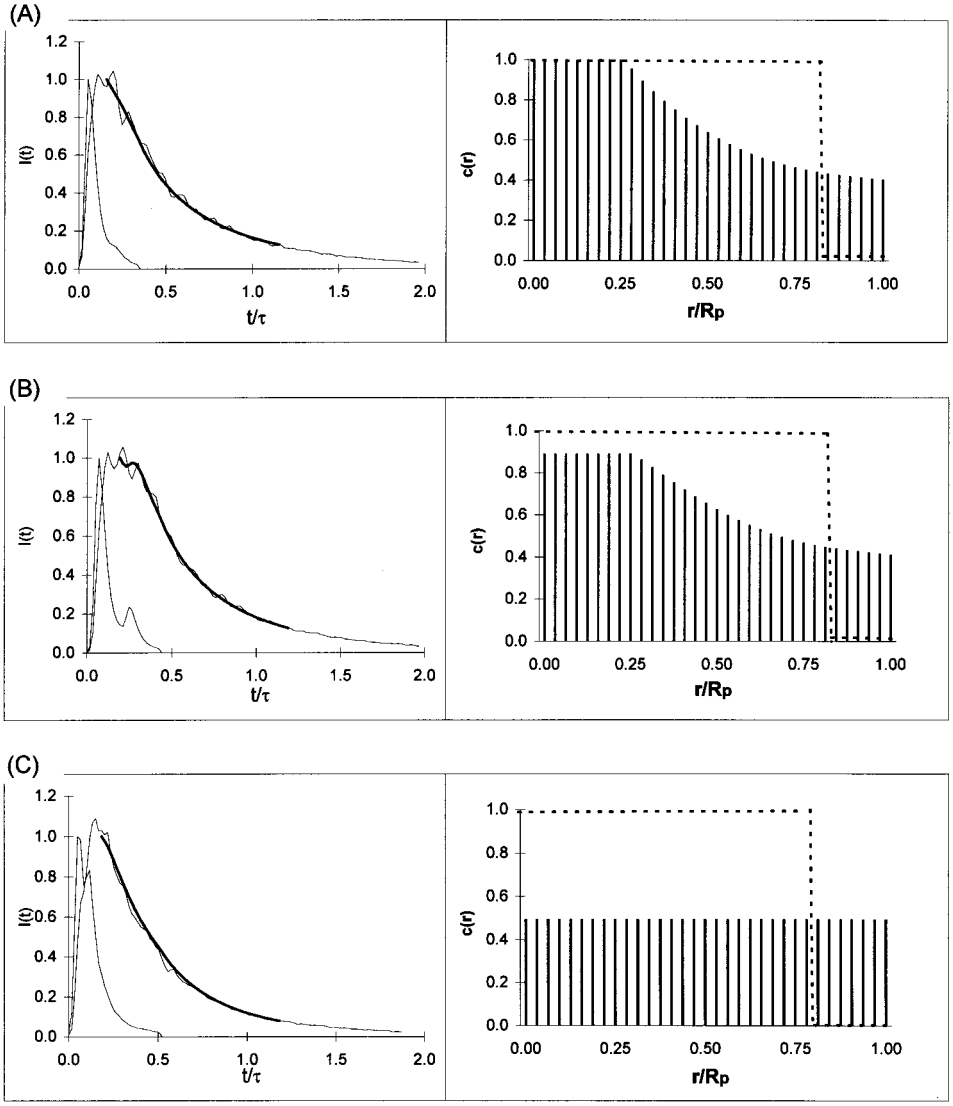

Figure 7. Latex particles CS4: (A) native; (B) annealed at 90 °C for 85 h; (C) film after dissolution in THF. Left-hand side: Experimental flash and experimental fluorescence decay. Bold: Region of the fluorescence decay where the least-squares and inversion procedure was applied. Right-hand side: Distribution profile of the donor-labeled polymer chains obtained with the least-squares and inversion procedure (vertical bars) and theoretical distribution corresponding to a perfect core−shell structure (dashed lines).

with $n_t = 56$ and $n_i = 33$, which gives $\nu = 23$. χ^2 is a quantity which is function of the quality of the fit of the fluorescence decay curve, obtained with the method of inversion, to the experimental curve. For a good adjustment χ^2 is close to 1. We also show in Table 1 the value, normalized, of the quantity (mass) of donors obtained by integration of the distribution curve. The ideal value of this quantity is 1. We see that at the end of the least-squares and inversion procedure the donor concentration is very close to 1.

A large discussion has been presented previously[11] concerning the origin of the internal structure of the latex studied here, based on the values of f'_A. This discussion is still valuable for these latexes, in spite of the fact that the values of f'_A and f_i reported in Table 1 are not identical. They are, however, pretty close from each other, and their variation follows the same trend when going from one system to another. It appears, therefore, that the earlier model, based on three distinct regions, gives reliable information on the degree of mixing of the core polymer and shell polymer inside the particles. The analysis of the decay curves with the method of inversion is, however, finer. For instance, in the cases where the fraction of mixing was found equal to 1 with f'_A, the values of f_i ranges between 0.8 and 1. In particular, for latexes CS4 native and CS4 annealed at 90 °C for 85 h, f_i is found equal to 0.909 and 0.922, respectively, while f'_A is equal to 1 in both cases. The increase of f_i between these two latexes is in agreement with the increase of the mixing of the polymer chains when the particles are annealed. However, the main advantage of the method of inversion is obviously that one gets, directly from the fluorescence decay curve, the distribution of the labeled polymer chains inside the particles. A last remark must be made concerning eventual aggregations between fluorophores. Aggregation between phenanthrene or between anthracene groups seems not to occur in our experiments. Indeed, for films prepared from dissolution of CS1 and CS2 in THF, we have compared the concentration C_0 calculated from eq 40, and the concentration C_0 calculated from the quantities of phenanthrene and anthracene added during the polymerization, assuming an homogeneous distribution, and the comparison is very satisfying, indicating nonaggregation between the fluorescent groups. On the other hand, annealing of latex CS2 at 140 °C leads to fraction of mixing as low as 0.15, indicating phase separation between phenanthrene labeled PBMA and anthracene-labeled PMMA.[11] This result shows that not much aggregation, if any, between phenanthrene and

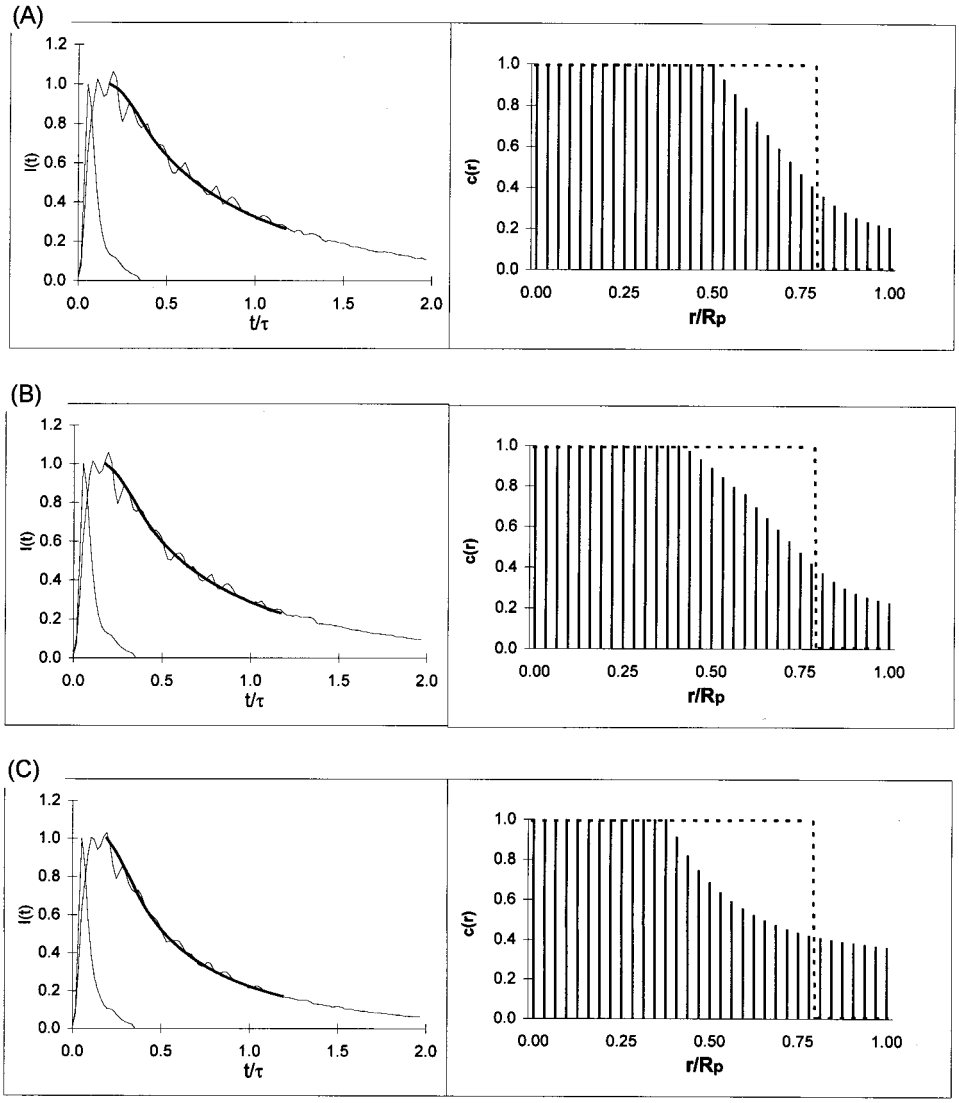

Figure 8. Latex particles CS2 (A), CS3 (B), and CS7 (C). Left-hand side: Experimental flash and experimental fluorescence decay. Bold: Region of the fluorescence decay where the least-squares and inversion procedure was applied. Right-hand side: Distribution profile of the donor-labeled polymer chains obtained with the least-squares and inversion procedure (vertical bars) and theoretical distribution corresponding to a perfect core−shell structure (dashed lines).

anthracene groups occurs; otherwise the fraction of mixing would have taken a value much larger than 0.15.

Conclusion

In this article, a method is described for the analysis of the fluorescence decay curves which leads to the distribution of the polymer chains labeled either with a donor or with an acceptor of energy, inside latex particles, without any model of distribution except the distributions of the donor and of the acceptor which were supposed radial and continuous. The donor is bonded to the chains which form theoretically the core of the particles, and the acceptors on the chains which form theoretically the shell. The distribution curves were compared with the distributions that one would have for perfect core−shell particles. In this work only acrylic polymers were studied, but the method can be employed to the study of other types of polymers. The method presented here is very appropriate to the study the influence of various parameters which may affect the internal structure of the particles. Determination of the polymer concentration profiles, as done here, can be helpful for the choice of the experimental conditions leading to some desired internal structure.

One can wonder if the inversion of the decay curve permits the distinction between different internal structures, for instance between a structure with a radial symmetry and a structure with inclusions of polymer domains in another polymer, the host polymer which forms the particle. One can easily imagine that in this last case a certain number of assumptions are necessary to interpret the decay curves such as, for example, to suppose that the interface between the inclusions and the polymer host is sharp, and that the inclusions are spherical and of the same size. It is only with the help of this type of assumptions that the method of inversion could be applied. However, the use of the method presented here to other systems is certainly possible. For instance, one can envisage to determine the distribution profiles of polymer chains in films formed by a mixture of latex particles labeled with a donor and with an acceptor of energy and compare the results given by our method with those which can be obtained with the method proposed by Winnik et al.,[18] or the distribution profile, in the interfacial region, of polymers belonging to different polymeric or composite materials brought into close contact. In this last case, interesting information could perhaps be obtained concerning certain mechanisms involved in the process of adhesion.

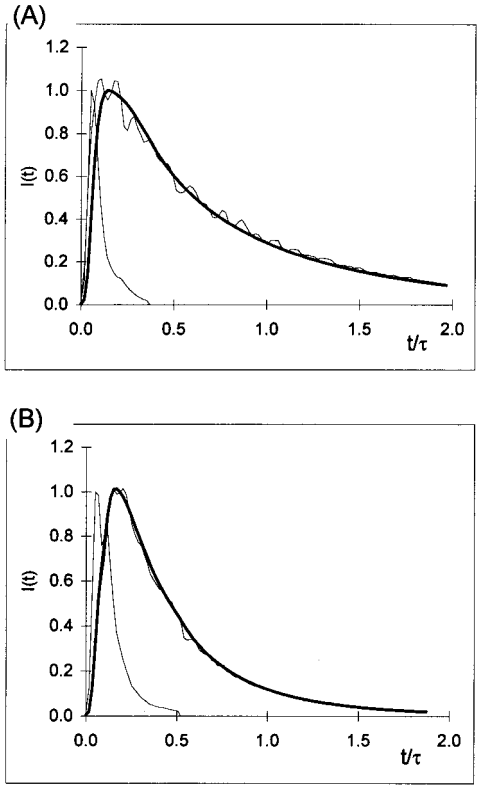

Figure 9. (A and B): Same systems as those presented in Figure 6, A and C, respectively. The curves in bold represent the decay curves recomputed, between $t = 0$ and $t = 2\tau$, from the concentration profile obtained after inversion.

Appendix

Here we present the functions which appear in the vector β_j (eq 19) and in the matrix α_{jk} (eq 21). The functions, b_j^0, b_j^1, and N_j^0, N_j^1 and are defined as

$$b_j^0 = \int_{t'_1}^{t'_2} K(t',c_j)\,\mathrm{d}t'$$

$$b_j^1 = \int_{t'_1}^{t'_2} qC_0\sqrt{t'}K(t',c_j)\,\mathrm{d}t'$$

$$N_j^0 = \frac{C_0}{N_\mathrm{D}}\int_i K_{ij}^0 r_i^2 4\pi\Delta r_i$$

$$N_j^1 = \frac{C_0}{N_\mathrm{D}}\int_i c_i K_{ij}^1 r_i^2 4\pi\Delta r_i$$

where t' is defined as $t' = t/\tau$, and the matrices K_{jk}^0 and K_{jk}^1 are defined as

$$K_{jk}^0 = \int_{t'_1}^{t'_2} \frac{1}{I_\mathrm{e}(t)} K(t',c_k)\,\mathrm{d}t'$$

$$K_{jk}^1 = \int_{t'_1}^{t'_2} \frac{1}{I_\mathrm{e}(t)} qC_0 K(t',c_j)K(t',c_k)\,\mathrm{d}t'$$

The matrix K_{jk}^2 used in the matrix α_{jk} are defined as

$$K_{jk}^2 = \int_{t'_1}^{t'_2} \frac{1}{I_\mathrm{e}(t)} q^2 C_0^2 K(t',c_j)K(t',c_k)\,\mathrm{d}t'$$

The time and spatial integration are calculated by the trapezoidal rule.

References and Notes

(1) (a) Kanig, G.; Neff, H. *Colloid. Polym. Sci.* **1975**, *253*, 29. (b) Misra S. C.; Pichot C.; El-Aasser, M. S.; Vanderhoff, J. W. *J. Polym. Sci., Polym. Lett. Ed.* **1979**, *17*, 567. (c) Misra S. C.; Pichot C.; El-Aasser, M. S.; Vanderhoff, J. W. *J. Polym. Sci., Polym. Chem. Ed.* **1983**, *21*, 2383. (d) Okubo, M.; Katsuta, Y.; Matsumoto, T. *J. Polym. Sci., Polym. Lett. Ed.* **1982**, *20*, 45. (e) Min, T. I.; Klein, A.; El-Aasser, M. S.; Vanderhoff, J. W. *J. Polym. Sci., Polym. Chem. Ed.* **1983**, *21*, 2845. (f) Chen, Y.-C.; Dimonie, V.; El-Aasser, M. S. *Macromolecules* **1991**, *24*, 3779. (g) Chen, Y.-C.; Dimonie, V. L.; Shaffer, O. L.; El-Aasser, M. S. *Polym. Int.* **1993**, *30*, 185. (h) Jönsson, J.-E.; Hassander, H.; Törnell B. *Macromolecules* **1994**, *27*, 1932. (i) He, W.; Tong, J.; Wang, M.; Pan, C.; Zhu, Q. *J. Appl. Polym. Sci.* **1995**, *55*, 667. (j) Hergeth, W.-H.; Bittrich, H.-J.; Eichhorn, F.; Schlenker, S.; Schmutzler, K.; Steinau, U.-J. *Polymer* **1989**, *60*, 1913. (k) Vandezande, G. A.; Rudin, A. *J. Coatings Technol.* **1994**, *66*, 99. (l) Kamei, S.; Okubo, M.; Masumoto, T. *J. Polym. Sci., Polym. Chem. Ed.* **1986**, *24*, 3109.

(2) (a) O'Reilly, J. M.; Melpolder, S. M.; Fischer, L. W.; Wignall G. D.; Ramakrishnan, V. *Polym. Prepr. (Am. Chem. Soc., Div. Polym. Chem.)* **1983**, *24* (2), 407. (b) Fischer, L. W.; Melpolder, S. M.; O'Reilly, J. M.; Ramakrishnan, V.; Wignall G. D., *J. Colloid Interface Sci.* **1988**, *123*, 24. (c) Wai, M. P.; Gelman, R. A.; Fatica, M. G.; Hoerl, R. H.; Wignall, G. D. *Polymer* **1987**, *28*, 918.

(3) Grunder, R.; Urban. G.; Ballauff, M. *Colloid Polym. Sci* **1993**, *271*, 563.

(4) (a) Dingenouts, N.; Ballauff, M. *Acta Polymer*. **1993**, *44*, 178. (b) Ballauff, M. *Macromol. Symp.* **1994**, *87*, 93.

(5) (a) Tembou Nzudie, D.; Delmotte, L.; Riess, G. *Makromol. Chem., Rapid Commun.* **1991**, *12*, 251. (b) Tembou Nzudie, D.; Delmotte, L.; Riess, G. *Macromol. Chem. Phys.* **1994**, *195*, 2723. (c) Spiegel, S.; Landfester, K.; Lieser, G.; Boeffel, C.; Spiess, H. W. *Macromol. Chem. Phys*. **1995**, *196*, 985. (d) Landfester, K.; Spiess, H. W. *Macromol. Rapid Commun.* **1996**, *17*, 875. (e) Landfester, K.; Boeffel, C.; Lambla, M.; Spiess, H. W. *Macromolecules* **1996**, *29*, 5972.

(6) Manzur, A. *J. Colloid Interface Sci.* **1994**, *162*, 197.

(7) Cavaillé, J. Y.; Jourdan, C.; Kong, X. Y.; Perez, J.; Pichot, C.; Guillot, J. *Polymer* **1988**, *27*, 693.

(8) Sommer, F.; Tran Min Duc; Pirri, R.; Meunier, G.; Quet, C. *Langmuir* **1995**, *11*, 440.

(9) (a) Dobler, F.; Pith, T.; Holl, Y.; Lambla, M. *J. Appl. Polym. Sci.* **1992**, *44*, 1075. (b) Muroi, S.; Hashimoto, H.; Hosoi, K. *J. Polym. Sci., Polym. Chem. Ed.* **1984**, *22*, 1365.

(10) Winnik, M. A.; Xu, H.; Satguru, R. *Makromol. Chem., Macromol. Symp.* **1993**, *70/71*, 107.

(11) Pérez, E.; Lang, J. *Langmuir* **1996**, *12*, 3180.

(12) Marion, P.; Beinert, G.; Juhué, D.; Lang, J. *Macromolecules* **1997**, *30*, 123.

(13) (a) Pekcan, Ö.; Winnik, M. A.; Croucher, M. D. *Macromolecules* **1990**, *23*, 2673. (b) Zhao, C.-L.; Wang, Y.; Hruska, Z.; Winnik, M. A. *Macromolecules* **1990**, *23*, 4082.

(14) Steinberg, I. Z. *J. Chem. Phys*. **1968**, *48*, 2411.

(15) (a) Förster, Th. *Ann. Phys. (Leipzig)* **1948**, *2*, 55. (b) Förster, Th. *Discuss. Faraday Soc*. **1959**, *27*, 7.

(16) Provencher, S. W.; Hendrix, J.; De Maeyer L. *J. Chem. Phys.* **1978**, *69*, 4273.

(17) (a) Liu, Y. S.; Ware, W. R. *J. Phys. Chem*. **1993**, *97*, 5980. (b) Liu, Y. S.; de Mayo, P.; Ware, W. R. *J. Phys. Chem*. **1993**, *97*, 5995.

(18) Liu, Y. S.; Li, L.; Ni, S.; Winnik, M. A. *Chem. Phys.* **1993**, *177*, 579.

(19) Demas, J. N. *Excited-State Lifetime Measurements*; Academic Press: New York, 1983.

(20) Tikhonov, A.; Arsenin, V. *Méthodes de Résolution de Problèmes Mal Posés*; Editions Mir: Moscow, 1976.

(21) Ahlberg, J.; Nilson, E.; Wolsh, J. *The Theory of Splines and Their Applications*; Academic Press: New York, 1967.

(22) Badeva, V.; Morazov, V. *Problèmes Incorrectement Posés*; Masson: Paris, 1991.

(23) Press, W. H.; Teukolsky, S. A.; Vetterling, W. T.; Flannery, B. P. *Numerical Recipes in C*; University Press: Cambridge, U.K., 1994.

(24) Conte, S. D.; de Boor, C. *Elementary Numerical Analysis*; McGraw-Hill International Book Company: Tokyo, 1982.

(25) see for exemple: Yule, G. U.; Kendall, M. G. *An Introduction to the Theory of Statistics*; Charles Griffin & Cia: London, 1950.

(26) Golub, G. H.; Van Loan, C. F. *Matrix Computation*; Johns Hopkins University Press: Baltimore, 1989.

(27) Carlaw, H. S.; Jaeger, J. C. *Conduction of Heat in Solids*; Clarendon Press: Oxford, U. K., 1986.

(28) Abramowit, M.; Stegun, I. A. *Handbook of Mathematical Functions*; Dover Publications: New York, 1972.